Progress in Oceanography 183 (2020) 102291

Contents lists available at ScienceDirect

Progress in Oceanography

journal homepage: www.elsevier.com/locate/pocean

Aerosol Fe cycling in the surface water of the Northwestern Pacific ocean

Bo-Shian Wang[a,b], Tung-Yuan Ho[a,c,*]

[a] Research Center for Environmental Changes, Academia Sinica, Taipei, Taiwan
[b] National Academy of Marine Research, Ocean Affairs Council, Kaohsiung, Taiwan
[c] Institute of Oceanography, National Taiwan University, Taipei, Taiwan

ARTICLE INFO

Keywords:
Iron
Aerosol
GEOTRACES
Suspended particle
Surface water, Northwestern Pacific Ocean

ABSTRACT

We investigated the transformation processes of aerosol Fe in the surface water of the Northwestern Pacific Oceanic region by comprehensively collecting and measuring aerosols, seawater, size-fractionated suspended particles, and sinking particles during seasonally representative low and high aerosol deposition months. With one order of magnitude higher aerosol Fe contributed to the surface ocean in the spring month, the elevated deposition of aerosols was not reflected in the dissolved pool but the suspended pool. Elemental ratios further indicate that biotic and abiotic suspended particulate Fe exhibited size-dependent distribution patterns. Lithogenic particles originating from aerosol deposition were mainly in particle fraction with sizes ranging from 2 to 25 μm in the surface water. Biotic particles smaller than 2 μm were the major carriers of intracellular and surface precipitated/aggregated Fe. Due to the relatively small size and low density of biotic particles, the surface precipitated/aggregated Fe on small biotic particles shall possess longer residence time and higher bioavailability than the large and dense lithogenic particles in the euphotic zone.

1. Introduction

The supply of iron (Fe) to oceanic surface water is a major factor controlling oceanic primary production and global carbon cycling (Martin et al., 1994). Aerosol deposition is a dominant process for supplying external Fe to the euphotic zone of the open ocean (Jickells et al., 2005; Baker and Croot, 2010). Due to their different chemical and physical properties, lithogenic or anthropogenic aerosol Fe may proceed with different transformation processes in the surface water after deposition. Lithogenic aerosols, possessing relatively large size and high density, are major aerosol Fe source in the surface water of the open ocean and have also been considered as the dominant soluble Fe source to the surface water in the North Atlantic Ocean or even globally (Duce and Tindale, 1991; Baker and Jickells, 2006). However, Fe solubility in mineral dusts is generally very low (Fung et al., 2000; Schroth et al., 2009). Comparatively, fine aerosols collected in remote oceanic areas possessed relatively high Fe solubility, indicating that relatively small size anthropogenic aerosols can be a significant source of soluble Fe to the surface ocean due to their high Fe solubility (Chuang et al., 2005; Schroth et al., 2009; Sholkovitz et al., 2012; Buck et al., 2013). Depositing to the surface water, either lithogenic or anthropogenic aerosol Fe would undergo a series of abiotic and biotic transformation processes, including dissolution and precipitation, adsorption and desorption, aggregation and disaggregation, suspension and sinking, and uptake and decomposition (Boyd et al., 2017; Tagliabue et al., 2017). These complicated physical and biogeochemical processes would then decide the retention time and bioavailability of aerosol Fe in the euphotic zone. The Fe availability would then influence phytoplankton growth and community structure, and subsequently carbon and major nutrient cycling in the ocean. However, the internal transformation processes of aerosol Fe in oceanic surface water still largely remain unclear (Boyd et al., 2017).

East Asia has accounted for about 70% of global coal consumption (http://www.iea.org/statistics/) and has emitted tremendous amount of anthropogenic aerosols to the adjacent oceanic regions (Myhre et al., 2009). Located downwind site of the strong northeastern monsoon in East Asia, the Northwestern Pacific Oceanic (NWPO) and its marginal seas thus receives large amounts of both anthropogenic and lithogenic aerosols during winter and spring, in contrast to extremely low aerosol deposition during summer and early fall by relatively weak southwestern monsoon (Matsui et al., 2013; Lin et al., 2015). Recent study showed that anthropogenic to lithogenic aerosol masses were up to one third in the NWPO oceanic region between 15–45°N and 125–150°E in 2010, where the estimated total aerosol deposition was up to 5.4×10^{10} kg yr^{-1} (Park et al., 2016). Large scale cross-basin field studies in the whole Pacific Ocean also observed that the NWPO region

* Corresponding author at: 128, Sec. 2, Academia Rd., Nankang, Taipei 115, Taiwan.
E-mail address: tyho@gate.sinica.edu.tw (T.-Y. Ho).

https://doi.org/10.1016/j.pocean.2020.102291
Received 1 March 2019; Received in revised form 5 December 2019; Accepted 4 February 2020
Available online 07 February 2020
0079-6611/

possessed the highest aerosol Fe fluxes, with averaged Fe fluxes to be 1.2 ± 1.3 (± SD) μmol m^{-2} d^{-1} and solubility to be 10 ± 5% at 30°N from 133°E to 160°E from June to August in 2004 (Buck et al., 2013). Model study showed that the annual aerosol Fe deposition rates of total and soluble Fe estimated were 2.2 and 0.09 mmol m^{-2} yr^{-1}, respectively, in the area between 20–25°N and 122–135°E of the NWPO (Lin et al., 2015). The feature of relatively high anthropogenic and lithogenic aerosol deposition fluxes with contrasting seasonality turns the NWPO into an ideal region to investigate the transformation and cycling processes of aerosol Fe in the surface ocean.

Through Taiwan GEOTRACES process study, we carried out two cruises during the representative periods of low and high aerosol deposition seasons, July 2013 and March 2014. We comprehensively determined Fe concentrations and fluxes in pools associated with aerosol Fe cycling in the surface water, including aerosols, seawater, size-fractionated suspended particles, and sinking particles, particularly emphasizing on investigating the transformation processes from aerosol Fe to size-fractionated suspended particulate Fe in the surface water of the NWPO.

2. Methods and material

2.1. Sampling and pretreatment

Aerosols, seawaters, suspended and sinking particles were collected on the R/V Ocean Research 5 along the 23.5°N latitudinal transect east off Taiwan toward 128°E during summer 2013 (OR5-1307, July 14–23) and spring 2014 (OR5-0035, March 25-April 03). There were total eight sampling stations in the two cruises. Only the data of the three most remote stations, Station 6, 7 and 8, were considered in this study, where the depths are deeper than 4500 m and the effects of river discharge, shelf sediment resuspension, and the Kuroshio may be ignorable (Fig. 1). Mesoscale eddies were monitored based on satellite derived sea surface height anomaly (Fig. S1). The frequent occurrence of mesoscale cold eddies in the NWPO is an important process upwelling subsurface water and transporting both major and minor nutrients to the euphotic zone (Benitez-Nelson et al., 2007). Beam attenuation coefficient (BAC) was measured by transmissometer during water sampling, which may be an indicator for particulate organic carbon or biomass in the surface water of the open ocean (Bishop, 1999) (Fig. 2A).

All the sampling and pretreatment procedures followed trace metal clean procedures referred to the recommended GEOTRACES protocols (http://www.geotraces.org/science/science-highlight/intercalibration/222-sampling-and-sample-handling-protocols-for-geotraces-cruises). Aerosol samples were collected on cellulose filters (Whatman W41) by total suspended particulate high volume air samplers at front deck of the vessel on the route of navigation. Seawater samples for dissolved trace metal analysis (0.5 L, triplicates) were collected by Teflon-lined GO-FLO samplers (General Oceanics) and filtered in a trace metal clean van using 0.2 μm acid cleaned filtered (PolyCap TC, Whatman). Size-fractioned suspended particles were filtered from unfiltered seawater (2L) within one hour after sample collection, using a vacuum pump (PTFE diaphragm pump, Büchi V-700) with pressure regulation (100 mm Hg) to prevent cell damage. Acid cleaned (1 N HCl) filter discs with sizes of 0.2 and 2 μm polycarbonate (Millipore), and 41 μm nylon (Millipore) were used during the summer 2013 cruise. We replaced the 41 μm nylon filter with 25 μm polyethylene (Millipore) to match the size range of lithogenic aerosols (Kurisu et al., 2016), which shall have limited influence on the results as our previous studies have shown about 90% of suspended particulate Fe within 0.2 and 10 μm (Ho et al., 2010; Liao et al., 2017). After sample filtration, additional 20 mL pure water was added and filtered for salt removal. Sinking particles were collected using custom made trace metal clean free floating traps at the depths of 50 m, 100 m, 150 m and 300 m at station 7 (July 2013) and station 6 (March 2014) for about 24 h (Ho et al., 2011). After retrieving traps, sinking particles were filtered and collected with 80 mm 0.2 μm polycarbonate membrane filters instantly in a trace metal clean bench on board.

2.2. Leaching and digestion

The solubility measurement of aerosol Fe was obtained by following the standard GEOTRACES protocol (Morton et al., 2013). Ultrapure HNO_3 (J.T. Baker ULTREX II) and double-distilled HF (sourced form J. T. Baker ULTREX II) were used for sample digestion. Aerosol total digestion was carried out by 5 mL 12 N HNO_3-6 N HF on a hotplate at 140 °C for 24 h. After 85 °C drying up, each digested sample was added 0.9 mL of 5 N HNO_3-3 N HCl, and digested at 85 °C again (closing lid) for 3-hour to remove calcium and magnesium fluoride. Each solution was added 1 mL 100 ppb Rh as internal standard, filled with H_2O to 10 mL, and filtered using a 0.2 μm cleaned PES filter disc. The digested samples were diluted 10 times with 0.3 N HNO_3 before elemental analysis. The averaged procedural Fe blank for digestion is 61 pg (n = 2). Most of the digestion procedures of suspended and sinking particles followed the method proposed in the study (Planquette and Sherrell, 2012). The suspended particle samples larger than 41 μm were digested with 1 N HNO_3-10% H_2O_2 to reduce external contamination from the nylon filters. Typical procedural Fe blank including filtration and digestion is less than 2 ng (n = 8).

2.3. Chemical analysis

Seawater samples for trace metal concentrations were pretreated with automated pretreatment protocols (Wang et al., 2014). The digested particulate Fe, aluminum (Al) and phosphorous (P) were analyzed by inductively coupled plasma mass spectrometry, with uncertainty better than 5% for all the three elements. The quality of sample preparation and instrumental analysis was monitored using the reference materials, including four 50 mL NASS-6 seawater for each station profile, and three 1 mg NIES28 for the three aerosol samples and the duplicates. The uncertainties observed in seawater and aerosol reference materials are better than 10% and 5% respectively. For accuracy validation, our laboratory has participated three GEOTRACES intercalibration practices, including GI04 and GP18 for dissolved trace metals and GEOTRACES particulate trace metal intercalibration. Our intercalibrated data of GI04 and GP18 have been accepted and reported in GEOTRACES IDP 2014 and 2017.

3. Results

3.1. Seasonal aerosol Fe concentrations and deposition

We carried out cruises in July 2013 and March 2014 in this study as July and March are well representative for the low and high aerosol deposition seasons in the oceanic region, respectively. The contrasting aerosol optical depths (AOD) observed during the sampling months validate that the two months of this study were well representative for the low and high aerosol deposition seasons (Fig. 1). The total and soluble concentrations of Fe, P, and Al in the aerosols collected during the two periods are shown in Table 1. The overall bulk aerosol Fe concentrations ranged from 0.77 to 0.85 and from 1.3 to 27 nmol m^{-3} for the summer and spring sampling periods, respectively, with averaged aerosol Fe concentration to be 12 ± 13 nmol m^{-3} (± SD) in the spring, 15 times of the summer concentration, 0.81 ± 0.04 nmol m^{-3} (± SD). The concentrations can be converted to dry deposition fluxes by using 0.99 cm s^{-1} as the deposition velocity (Young and Silker, 1980), which result in the fluxes to be 0.69 ± 0.03 and 10 ± 12 μmol m^{-2} d^{-1} for the summer and the spring sampling period, respectively. Previous modeling study also reported that aerosol Fe deposition was 9 times higher in spring than summer in the subtropical NWPO (Lin et al., 2015). In terms of aerosol Fe solubility, the averaged aerosol Fe solubility observed in the low and high seasons

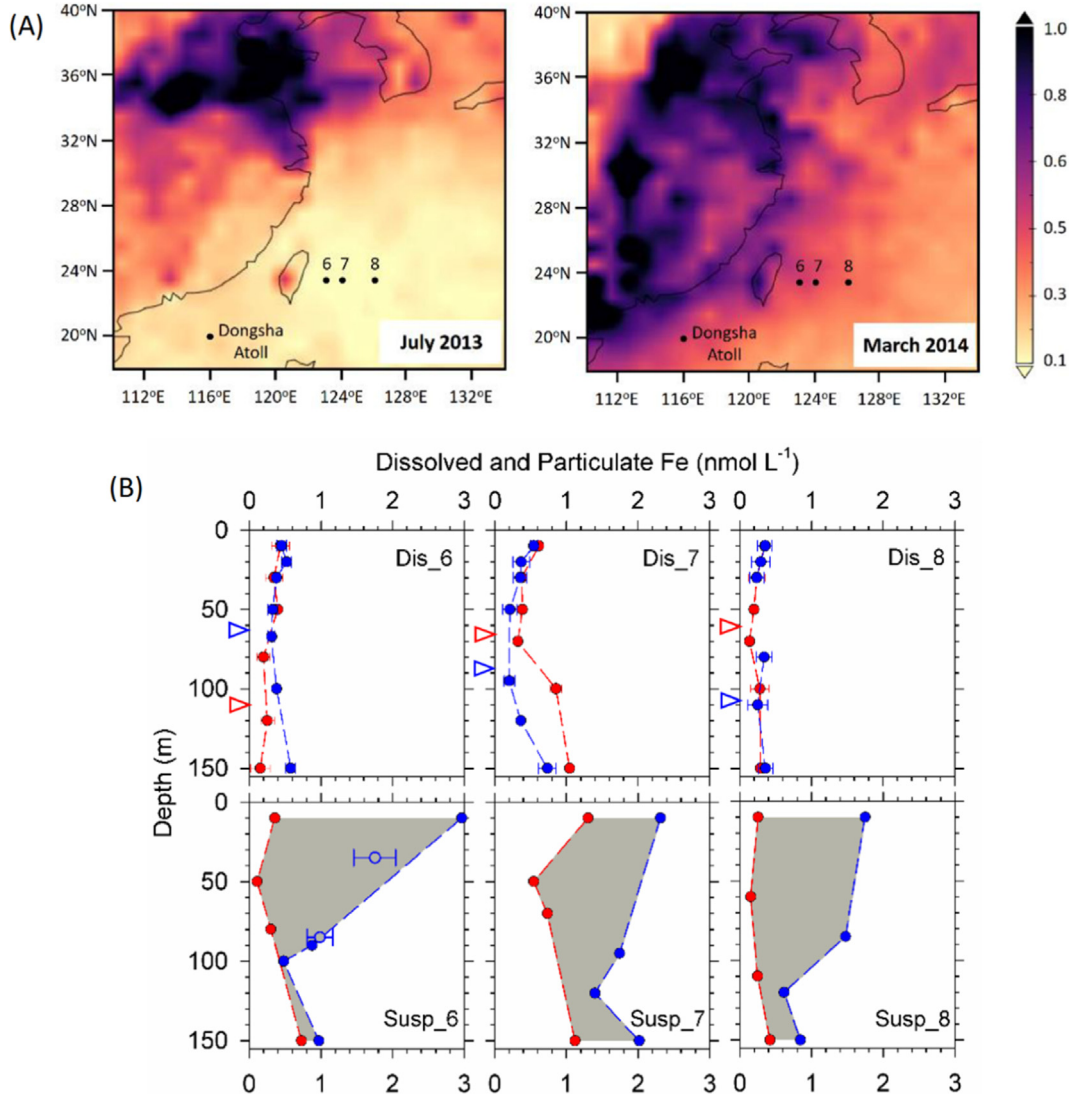

Fig. 1. (A) Monthly mean aerosol optical depth (AOD) in July 2013 and March 2014 acquired from MODIS-Aqua at 550 nm (http://giovanni.gsfc.nasa.gov). Field sampling stations 6, 7 and 8 and Dongsha Atoll Research Station are marked. (B) Vertical profiles of dissolved (Dis) and suspended particulate (Susp) Fe concentrations in the upper 150 m at station 6, 7 and 8 in the summer (red circle) and spring (blue circle) sampling seasons. Error bars for the dissolved and replicate suspended particulate Fe are one standard deviation. Replicate sampling (open circle) was conducted at station 6 in the spring for accuracy validation. Grey areas indicate the differences in suspended Fe concentrations between the high and low aerosol deposition seasons. Chlorophyll *a* maximum depths for the two occasions are indicated by triangles on the y-axis profiles. (For interpretation of the references to color in this figure legend, the reader is referred to the web version of this article.)

were 16 ± 3 and 11 ± 4%, respectively (Table S1), similar to the value reported in previous field study in the NWPO (9 ± 8%) (Buck et al., 2006).

3.2. Dissolved Fe concentrations

Although the overall dissolved Fe concentrations varied from 0.14 to 1.05 nmol L^{-1} in the surface water of the three remote stations (Fig. 1B and Table S2), the differences of dissolved Fe concentrations were generally seasonally insignificant. The dissolved Fe data from station 8, the most offshore station in this study, was vertically and seasonally comparable within the upper 150 m. The averaged dissolved Fe in the surface water at station 8 was 0.28 ± 0.07 nmol L^{-1} (± SD), similar to those reported in previous studies in the North Pacific Ocean (Johnson et al., 2003; Wu et al., 2011). The dissolved Fe concentrations at station 6 were also comparable among the two seasons except the slightly higher concentrations at 150 m in spring, 0.58 ± 0.07 nmol L^{-1}. However, the dissolved Fe profiles at station 7 display relatively large vertical and seasonal variations, which vary from 0.38 to 1.05 nmol L^{-1} and 0.21 to 0.74 nmol L^{-1} for the summer and spring, respectively. These subsurface high dissolved Fe observed at station 7 was likely attributed to cold eddy effect (Figs. S1 and S2), supported by the consistent variation patterns of hydrographic parameters and major nutrients observed (Table S2).

3.3. Fe and elemental ratios in suspended particles

Three different size-fractionated suspended particles were collected in this study, including the small fraction with size between 0.2 and 2 μm, the medium fraction with size from 2 to 41 or from 2 to 25 μm, the large fraction with size larger than 41 (or 25) μm. For the spring cruise, we changed the filter pore size from 41 to 25 μm for the medium fraction to match lithogenic aerosol size range closely (Takahashi et al., 2011). During the high aerosol deposition period, the suspended particulate Fe concentrations were significantly elevated in both bulk and size-fractionated particles at all stations, particularly at the very surface

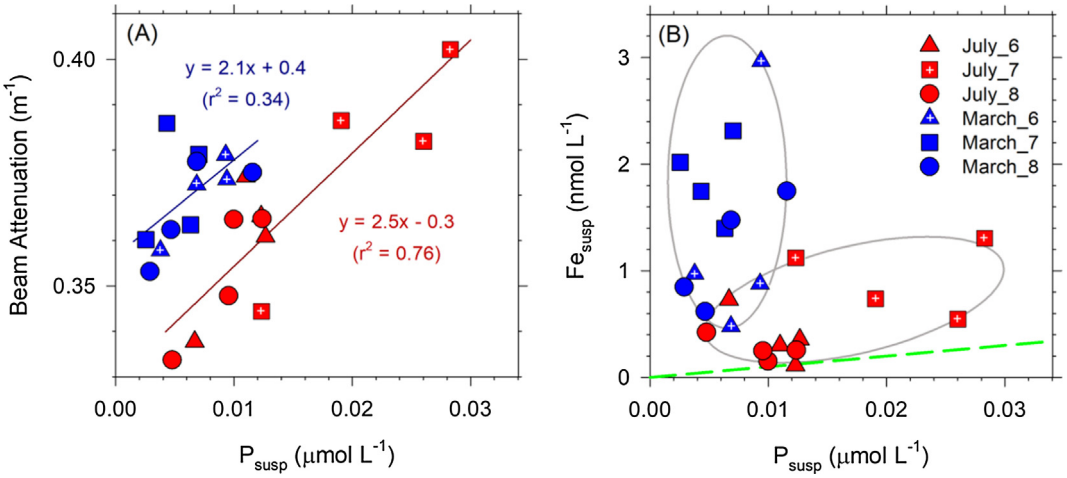

Fig. 2. (A) Linear regression between beam attenuation coefficient (BAC) and total suspended particulate P concentrations in the summer (red symbols) and spring (blue symbols) at station 6 (triangle), 7 (square) and 8 (circle). Symbols with white cross indicate stations close to the center of a cold eddy. (B) The comparison of suspended particulate Fe and P concentrations. The green dash line is intracellular Fe/P ratio, 7.5 mmol mol^{-1} (Ho et al., 2003). (For interpretation of the references to color in this figure legend, the reader is referred to the web version of this article.)

depths (Figs. 1, 2B and S3, and Table 2). In terms of Fe concentrations among the three size fractions, the medium size particles were the dominant fraction. Overall, the Fe concentrations were 179 ± 181 (0.2–2 μm), 336 ± 354 (2–41 μm), and 10 ± 8 pmol L^{-1} (> 41 μm) for the summer samples, and 519 ± 260 (0.2–2 μm), 738 ± 339 (2–25 μm), and 198 ± 278 pmol L^{-1} (> 25 μm) for the spring samples (mean ± SD). The Fe concentrations of the fine and medium fractions combined accounted for 98 ± 1% of total particulate Fe in the summer and 86 ± 10% in the spring (Table 2).

In contrast to the seasonally comparable dissolved Fe concentrations observed in the surface water, the total suspended particulate Fe concentrations in the upper 100 m-depth at each station were significantly higher in the spring than the summer period ($p < 0.01$; Figs. 1B and 2B). The overall mean total suspended particulate Fe were 0.52 ± 0.35 and 1.45 ± 0.74 nmol L^{-1} for the summer and the spring sampling period (Table S1). The depths with highest particulate Fe concentrations were all located in the very surface depth during the spring sampling period, indicating the top-down input from aerosol deposition. Similar to the dissolved concentrations observed at St. 7 at the summer sampling period, the suspended particulate Fe concentrations were about 2 times higher than the adjacent stations (Fig. 1B), which was also likely attributed to the cold eddy effect (Figs. S1 and S2).

Since P- or Al-normalized metal ratios are highly distinguishable among biogenic, lithogenic, and anthropogenic particles, the elemental ratios in the particles are useful to evaluate the relative contribution of various biotic and abiotic particles to the total particulate metal concentrations by comparing the ratios to the reference ratios of original sources. Using the elemental ratio information, our previous studies demonstrated that anthropogenic aerosol deposition was the major source of most particulate trace metals in the surface water of the NWPO and its marginal seas (Ho et al., 2010; Liao et al., 2017). Here, we have used similar approach to elucidate the sources and composition of particulate metals in particle samples collected in this study.

Particulate P is a reliable biomass proxy in the surface water of the open ocean as abiotic particulate P accounts for a very small portion in the surface water. For more than 90% of the samples collected in this study (Table 2), lithogenic P only account for less than 1% of total particulate P concentrations by using the particulate Al data and 0.01 as lithogenic P to Al molar ratio for estimate (Wedepohl, 1995). The concentrations of total suspended particulate P generally ranged from 2 to 12 nmol L^{-1} for the majority of the data except the three elevated data points obtained at St. 7 at the summer time, which were up to 28 nmol L^{-1} (Fig. 2A and Fig. S3). The elevated concentrations were likely attributed to the cold eddy effect (Fig. S1 and S2). The summer particulate P concentrations exhibits strong linear correlation with BAC ($r^2 = 0.76$, n = 12, $p < 0.05$), validating the dominance of biotic

Table 1
Concentrations and solubility (%) of Fe, P and Al (mean ± average deviation, n = 2) in aerosols and elemental vertical fluxes obtained from particle sinking at 150 m-depth during the two sampling seasons.

Element	Station	Aerosol concentration (nmol m^{-3}) [a] & Solubility				Particle$_{sink}$ (μmol m^{-2} d^{-1})	
		Summer	Sol. (%)	Spring	Sol. (%)	Summer	Spring
Fe	6	0.80 ± 0.01	18	1.3 ± 0.1	11		5.4 ± 1.7
	7	0.77 ± 0.1	13	27 ± 5	7	11 ± 6.0	
	8	0.85 ± 0.01	18	7.4 ± 1.1	15		
Average		**0.81 ± 0.04**	**16**	**12 ± 13**	**11**		
P	6	0.12 ± 0.01	100	0.07 ± 0.05	64		5.6 ± 3.3
	7	0.08 ± 0.01	100	1.3 ± 0.05	57	21 ± 1.2	
	8	0.11 ± 0.03	100	0.5 ± 0.05	75		
Average		**0.10 ± 0.02**	**100**	**0.61 ± 0.60**	**65**		
Al	6	3.3 ± 0.4	2	5.3 ± 0.6	9		6.8 ± 3.4
	7	3.2 ± 0.01	4	98 ± 4	4	15 ± 6.1	
	8	2.1 ± 0.09	5	28 ± 0.2	8		
Average		**2.9 ± 0.67**	**4**	**44 ± 48**	**7**		

[a] Aerosols were collected from July 19 to 21 in 2013, and from March 28 to April 01 in 2014, respectively.

Table 2
The concentrations of size-fractionated suspended particulate Fe, P, and Al.

	Depth	Fe (pmol L^{-1})			P (nmol L^{-1})			Al (nmol L^{-1})		
		OR5-1307 (Summer)[a]								
	(m)	0.2–2	2–41	> 41	0.2–2	2–41	> 41	0.2–2	2–41	> 41
St.6	10	77	272	6.5	11	1.2	0.8	0.5	2.0	0.1
	50	18	90	4.4	9.7	1.6	0.9	0.4	0.6	0.03
	80	56	243	3.8	8.2	1.5	1.3	0.5	1.1	0.02
	150	406	322	1.5	5.7	0.8	0.2	0.8	0.8	0.1
St.7	10	163	1135	4.9	18	5.4	4.9	0.2	3.2	0.1
	50	136	381	31	21	3.3	1.7	0.1	1.7	0.4
	70	666	53	17	18	0.7	0.8	3.8	0.5	0.1
	150	149	973	n.a.[b]	11	1.2	0.5	0.5	3.8	0.01
St.8	10	121	120	15	8.8	1.4	2.1	0.4	1.0	0.01
	60	69	75	6.6	9.2	0.7	0.2	0.2	0.3	0.01
	110	145	97	6.5	7.5	1.3	0.7	0.2	0.5	n.a.[b]
	150	141	271	10	3.9	0.6	0.3	0.5	1.2	0.02
		OR5-0035 (Spring)[a]								
		0.2–2	2–25	> 25	0.2–2	2–25	> 25	0.2–	2–25	> 25
St.6	10	772	1152	1041	4.8	1.5	3.1	0.9	2.8	1.8
	90	239	485	153	5.4	1.3	2.6	0.4	0.7	0.7
	100	159	251	69	4.3	1.2	1.3	0.2	0.7	0.7
	150	203	696	73	2.0	0.8	0.9	0.4	2.0	0.9
St.7	10	875	1291	146	5.2	1.1	0.7	4.9	6.4	1.2
	95	585	1096	63	3.0	0.7	0.7	5.3	3.4	0.9
	120	627	712	60	4.5	0.9	1.0	3.1	3.3	0.7
	150	764	902	351	1.7	0.3	0.5	5.0	4.2	1.6
St.8	10	729	887	131	9.5	0.9	1.2	4.1	3.4	0.8
	85	666	676	134	5.4	0.7	0.7	2.4	2.5	1.2
	120	237	300	80	3.5	0.6	0.5	2.2	2.1	0.7
	150	367	409	71	1.9	0.5	0.6	2.5	2.3	1.1

[a] The unit for all particle sizes is μm. Aerosols were collected from July 19 to 21 in 2013, and from March 28 to April 01 in 2014, respectively.
[b] n.a.: Not available, below detection limit.

particles in the suspended particles during the summer period (Fig. 2A). However, the correlation coefficient between BAC and particulate P was lower at the spring time (r^2 = 0.34, n = 12, $p < 0.05$) than the summer period. It can be attributed to the increasing abiotic or lithogenic aerosol particle input during the high deposition season. Indeed, the Fe/P ratios in the March period were 6.3-fold of the value observed in the July period. The Fe to P ratios in total suspended particles ranged from 70 to 793 mmol mol^{-1} in the spring sampling period, with an average of 273 ± 192 mmol mol^{-1}, in comparison with the value ranging from 9.1 to 109 in the summer sampling period, with an average of 43 ± 34 mmol mol^{-1} (Fig. 3A).

Elemental concentrations in size-fractionated particles show that the dominant particulate P or biotic particles was in the smallest fraction, accounting for 81 and 67% of the total particulate P for the summer and spring periods, respectively (Table 2). This result is expected because the dominant phytoplankton group is *Prochlorococcus* in the NWPO (Partensky et al., 1999). However, the dominant particulate Fe fraction was the medium fraction, accounting for 66 and 52% for the summer and spring periods, in comparison with 32 and 36% in the small fraction, respectively (Table 2; Fig. S3). The mismatch between major particulate Fe and P fractions indicates that most of particulate Fe was not associated with biogenic particles but existed as independent abiotic particles. The size of the dominant abiotic particulate Fe fraction agrees with the dominant aerosol size collected in Eastern China and Japan, that over 80% of Fe-containing lithogenic aerosols with sizes ranging from 2 to 10 μm (Takahashi et al., 2011). The size consistency indicates that the majority of aerosol deposited stayed as suspended particles with size similar to lithogenic aerosols in the surface water.

In terms of elemental ratios, a unique distribution pattern was observed for both the low and high aerosol deposition seasons (Fig. 3). Fe

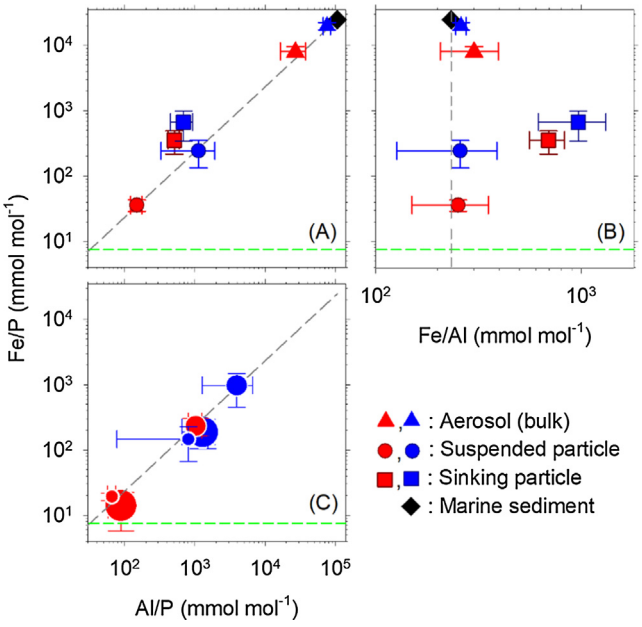

Fig. 3. The distribution patterns of total particulate elemental ratios (Fe/P vs. Al/P and Fe/Al) for the aerosols (triangle), suspended (circle) and sinking (square) particles in the summer (red symbols) and spring (blue symbols) sampling seasons (A) and (B). The ratios for aerosols and suspended and sinking particles are represented by the mean of the three stations with one standard deviation (± SD). Phytoplankton intracellular Fe/P ratio and upper crustal Fe/Al (192 mmol mol^{-1}) (Wedepohl, 1995) are shown in green and grey dash lines, respectively. The averaged Fe/P and Al/P of the local marine surface sediments (black diamond) (Bentahila et al., 2008) is shown in (A). The size-fractionated suspended particulate Fe/P and Fe/Al are shown in (C). The small, medium, and large circles stand for the small, medium, and large fractions of the size-fractionated particles. (For interpretation of the references to color in this figure legend, the reader is referred to the web version of this article.)

to P ratios in the medium fraction were about one order of magnitude higher than the small and large fractions for both sampling seasons. The ratios were 19 ± 20 and 146 ± 108 (small), 233 ± 227 and 971 ± 635 (medium), and 14 ± 13 and 188 ± 201 (large) mmol mol^{-1} for the summer and spring data in the small, medium and large fractions, respectively (Fig. 3C and S4). For both the small and large fractions obtained in the low aerosol sampling period, the averaged Fe to P ratios, 18 ± 20 and 14 ± 13 mmol mol^{-1}, were comparable to the proposed intracellular Fe quota (Ho et al., 2003; Ho, 2006), indicating that the particulate Fe were mainly intracellular in the two fractions. However, the Fe/P ratios of the small and large fractions in the spring period, 146 ± 108 and 188 ± 201 mmol mol^{-1}, were at least one order of magnitude higher than the intracellular ratios. Estimated by particulate P concentrations and the intracellular Fe to P ratios, the intracellular Fe in the small and large fractions only account for 8.0% and 7.1% of the total suspended Fe, indicating that more than 90% of the particulate Fe observed in spring was either independent abiotic particles or extracellularly aggregated or adsorbed fraction in the small and large fractions. With relatively large surface area, Fe in small fraction accounted for 32 and 36% of the total suspended Fe, in comparison with 2.6% and 12% in larger fraction for summer and spring periods, respectively (Fig. S3).

3.4. Fe fluxes of sinking particles

Sinking particles were collected at stations 7 and 6 during the summer and spring cruises, respectively. Microscopic and chemical analyses show that the sinking particles were mainly composed of biogenic particles, including planktonic carcasses and debris, fecal pellets, and a small portion of carbonate shells (Fig. S5). With

increasing suspended particulate concentrations observed in the high aerosol deposition period, we expect to observe elevated sinking particle fluxes in the spring sampling period like elevated aerosols deposition and suspended particles. However, the Fe fluxes observed by the traps deployed at St. 6 in the spring sampling period were 5.4 ± 1.7 μmol m^{-2} d^{-1}, lower than the flux observed at St. 7 in the summer sampling period, which was 11 ± 6.0 μmol m^{-2} d^{-1} (Table 1). It should be particularly mentioned that, unlike the aerosols and suspended particles sampling covering all stations, sinking particle sampling by floating traps was carried out at one station in each cruise due to the limitation of cruise time. As pointed out previously, St. 7 and its adjacent region encountered a strong cold eddy event during the summer sampling period (Fig. S1). The enhanced primary production and elevated biomass observed at St. 7 may explain the abnormally high sinking particle fluxes observed at the summer sampling time. As eddies are frequently formed in the NWPO region, material cycling can be strongly influenced by the physical process in the surface water of the oceanic region (Chen et al., 2013; Shih et al., 2015).

4. Discussion

4.1. Aerosol Fe fluxes and seasonal variations

The contrasting seasonality of aerosol deposition fluxes in the NWPO in the two major monsoon seasons were well documented, high deposition during strong northeastern monsoon seasons in winter and spring and extremely low deposition during weak southwestern monsoon seasons in summer and early autumn (Duce and Tindale, 1991; Uematsu et al., 2003). A case model study also reported that the total aerosol Fe fluxes were 1.3 and 11 μmol m^{-2} d^{-1} for summer and spring in the NWPO, respectively (Lin et al., 2015). Black carbon concentrations in spring was 5 times of the value observed in summer in the NWPO (Matsui et al., 2013). Similarly, the dry aerosol Fe fluxes observed in this study were 0.69 ± 0.03 and 10 ± 12 μmol m^{-2} d^{-1} during the summer and spring sampling periods, respectively. The total aerosol Fe fluxes were about 1.2 and 17 μmol m^{-2} d^{-1} for the two sampling periods by assuming 60% of dry aerosol Fe deposition to the total deposition in the NWPO (Uematsu et al., 2003; Ho et al., 2010). The averaged dry aerosol Fe solubility observed in this study were 16 ± 3 and 11 ± 4% in the low and high seasons, respectively, which are significantly higher than lithogenic aerosol Fe solubility reported previously, generally around 1% or less (Sholkovitz et al., 2012). The relatively high aerosol Fe solubility in our studied region appears to be attributed to the high percentage of anthropogenic aerosols (Kurisu et al., 2016; Park et al., 2016). Our new data in the South China Sea also show that the averaged PM 2.5 Fe solubility, mainly composed of anthropogenic aerosols, was up to 45% (Ho et al., 2018). Using the solubility (16% and 11%) and total flux data (1.2 and 17 μmol m^{-2} d^{-1}) obtained in this study, the total estimated soluble Fe fluxes would be 0.18 and 1.9 μmol m^{-2} d^{-1} for the summer and spring. Relatively, Lin et al. (2015) showed the deposition of soluble aerosol Fe were 3.4 times higher in spring (0.41 μmol m^{-2} d^{-1}) than in summer (0.12 μmol m^{-2} d^{-1}) in the NWPO by assuming that Fe solubility of 0.45% in mineral dust and 40% in anthropogenic aerosols. Buck et al. (2013) also observed comparable Fe deposition flux in 2004 summer, 0.20 ± 0.23 μmol m^{-2} d^{-1}, by using soluble Fe solubility of 10 ± 5% obtained in the NWPO region (133–158°E, 30°N).

To carry out a preliminary estimate for annual aerosol Fe fluxes, we first simply assume that the fluxes obtained during the summer and spring periods may represent the averaged fluxes for the low and high deposition seasons for 6 months each. Using AOD as aerosol and total Fe concentration index (Fig. S6), we found that the two fluxes extrapolated to 6 month period were close to the AOD value, showing only 9% difference to the AOD index. The annual aerosol total and soluble Fe fluxes roughly estimated are 3345 and 378 μmol m^{-2} yr^{-1}, respectively. The annual soluble Fe flux is significantly higher than the flux estimated by model studies. Luo et al. (2008) reported the flux to be 42 μmol m^{-2} yr^{-1} on the same region by assuming the Fe solubility to be 0.4% for mineral and 4% for anthropogenic aerosols; Lin et al. (2015) reported the flux to be 88 μmol m^{-2} yr^{-1} by using 0.45 and 40% as Fe solubility in lithogenic and anthropogenic aerosols, respectively. The discrepancy of the fluxes may be attributed to the different Fe solubility used in the model studies, either for lithogenic or anthropogenic aerosols (Kurisu et al., 2016; Conway et al., 2019). As Fe solubility differentiates and varies significantly between anthropogenic and lithogenic aerosols, it is essential to separate the two different types of aerosols in future studies to accurately estimate soluble aerosol Fe sources and fluxes in the surface ocean globally.

4.2. Seasonally comparable dissolved Fe concentrations

Despite of high aerosol Fe flux observed in the spring sampling period, dissolved Fe concentrations observed remained generally comparable among the two sampling periods in the upper 150 m of the studied region (Fig. 1B). The inconsistency between the highly varied aerosol deposition fluxes and the comparable dissolved Fe concentrations suggests that the major controlling factor for soluble Fe concentrations in the oceanic region is not external Fe input but likely to be the availability of Fe binding organic ligands (Hunter and Boyd, 2007). Theoretically, without the complexation of Fe organic ligands, Fe solubility in seawater would be down to low picomolar level or lower (Liu and Millero, 2002). Lacking of organic ligand concentrations, soluble aerosol Fe would precipitate as iron oxides or oxy-hydroxides shortly after deposition and be rapidly scavenged by ambient suspended particles (Fitzsimmons and Boyle, 2014). We propose that the comparable dissolved Fe concentrations observed during the two sampling seasons are attributed to limited available Fe binding organic ligands in the surface water. Indeed, the averaged dissolved Fe concentration in the surface water of St. 8 was 0.28 ± 0.07 nmol L^{-1}, which is comparable to the reported dissolved Fe in surface waters of the Pacific Ocean, 0.20 ± 0.13 nmol L^{-1} (Brown et al., 2005; Hansard et al., 2009), of the tropical eastern Atlantic Ocean, 0.28 ± 0.21 nmol L^{-1} (Sarthou et al., 2003), and of the Southern Ocean, 0.18 ± 0.08 nmol L^{-1} (Schlitzer et al., 2018) (Table S1). Using the data reported in GEOTRACES IDP 2017 (Schlitzer et al., 2018), the global average dissolved Fe concentration in the upper 150 m would be 0.26 ± 0.16 nmol L^{-1}. These comparable dissolved Fe concentrations suggest that the available concentrations of Fe binding organic ligands may be an important factor on deciding dissolved Fe concentrations in the surface waters globally.

4.3. Elevated Fe/P ratios in suspended and sinking particles of the surface water

The positive correlation between increasing aerosol deposition and elevated Fe to P ratios observed in the suspended particles (Fig. 3) support our previous argument that elevated trace metal ratios in size-fractionated plankton or particles was mainly attributed to aerosol deposition in the surface water of the NWPO and its marginal seas (Ho et al., 2007; Liao et al., 2017). Here, we further compiled the data of Fe to P ratio in suspended particles collected in the surface water of the global ocean and compared them with atmospheric aerosol concentrations. We also found positive correlation patterns between atmospheric aerosol concentrations and Fe to P enrichment ratios globally (Fig. 4). Biological enrichment factors are obtained by using particulate Fe to P ratios divided by intracellular Fe to P ratios. As dissolved Fe concentrations are relatively comparable in the surface water of the open ocean globally, generally ranging from 0.1 to 1.0 nmol L^{-1}, with an overall average to be 0.31 ± 0.12 nmol L^{-1} (Table S1), the highly elevated Fe to P ratios observed are unlikely attributed to biological uptake but to elevated abiotic particles or extracellularly aggregated Fe on biotic particles. In addition to high value observed in the NWPO

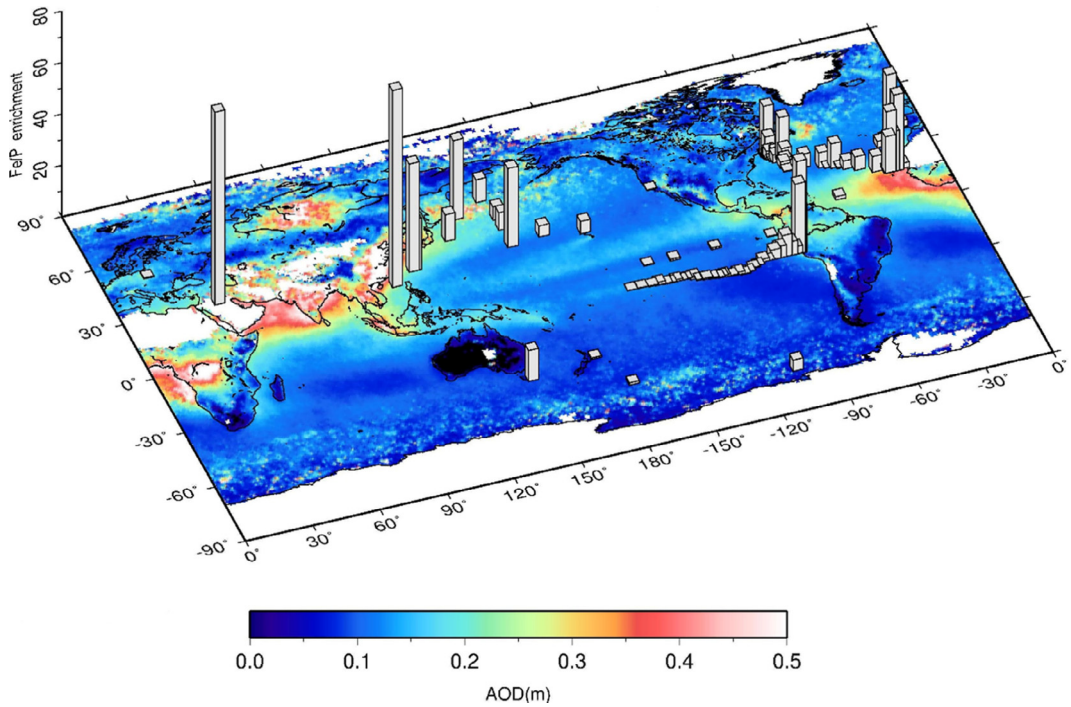

Fig. 4. The comparison of Fe/P biological enrichment factors and AOD in the global surface ocean. The annual averaged AOD are derived from MODIS-Aqua at 550 nm from 2007 to 2017. The biological enrichment factors are obtained by using reported suspended particulate Fe/P data divided by the intracellular Fe/P quota, 7.5 mmol mol^{-1} (Ho et al., 2003; Ho, 2006). The suspended particulate Fe/P data used in this figures include the following studies (Martin and Knauer, 1973; Collier and Edmond, 1984; Weinstein and Moran, 2004; Tovar-Sanchez et al., 2006; Ho et al., 2007; Bowie et al., 2010; Morton, 2010; Twining et al., 2011; Yiğiterhan et al., 2011; Nuester et al., 2012; Planquette et al., 2013; Wilhelm et al., 2013; Lam et al., 2015; Twining et al., 2015; Twining et al., 2016; Liao et al., 2017).

regions, elevated enrichment factors were also observed in the surface water of the regions near the eastern and western ends of the North Atlantic Ocean and the eastern end of the Southeastern Pacific Ocean, where the aerosol optical depths are relatively high (Lam et al., 2015; Sherrell et al., 2016). Contrarily, the lowest values shown are located in the non-upwelling open ocean region in the Southeastern Pacific Ocean, where aerosol concentrations are extremely low.

In comparison with intracellular Fe/P ratio and lithogenic Fe/Al ratios, we also observe elevated Fe ratios in the sinking particles (Fig. 3). The averaged Fe to P ratios in the sinking particles were 353 ± 137 and 666 ± 324 mmol mol^{-1} for the summer and spring sampling periods, respectively (Fig. 3A), which was insignificantly different ($p = 0.34$). These values are about 2 orders of magnitude of Fe intracellular quota (Ho et al., 2003). As fecal pellets and marine snow were dominant components in the sinking particles (Fig. S5), the elevated Fe to P ratios in sinking particles may reflect preferential aggregation of abiotic particles on the organic particles (Bowie et al., 2015), and/or preferential degradation of particulate organic P (Faul et al., 2005). The possible sources causing the elevated Fe/P and Fe/Al ratios may be contributed from anthropogenic aerosols, authigenic particles, and adsorption and aggregation of Fe on biotic particles.

4.4. Aerosol Fe transformation processes in the surface water

Based on the observation of this study, we may try to compile and quantify the inventories of major Fe pools and fluxes in the top 150 m of the studied region (Fig. 5). The total aerosol deposition fluxes were 1.2 and 17 μmol m^{-2} d^{-1} for the summer and spring seasons, respectively. In terms of sinking particle fluxes, the enhanced Fe sinking flux during the summer period mainly reflected the short term eddy effect and was substantially overestimated for the whole season, which are not presented and discussed. The bottom up fluxes of dissolved Fe to the surface water may be indirectly estimated by nitrate fluxes. Previous study estimated bottom up nitrate flux in the surface water of the NWPO by assuming the upward nitrate flux to be balanced by exported particulate organic nitrogen (PON) under steady state condition (Hirose and Kamiya, 2003). Assuming mass balance between upwelled nitrate flux and PON sinking flux in the studied region, an averaged PON export (or nitrate upwelling) of 0.77 mmol m^{-2} d^{-1} can be derived by using the reported POC fluxes obtained in the NWPO (Hirose and Kamiya, 2003; Chen et al., 2013; Shih et al., 2015). The calculated PON export or upwelling nitrate flux also agrees with the value estimated by seawater vertical mixing and diffusivity obtained in this study. Using 6 mmol mol^{-1} as dissolved Fe to nitrate ratio in the upwelled water (Fung et al., 2000), the estimated dissolved Fe flux from the subsurface layer to the top 150 m zone was only 0.11 μmol m^{-2} d^{-1} for the spring in the NWPO (Table S2). This bottom up Fe flux accounted for about 7% of the aerosol Fe flux in summer time and was ignorable in comparison to the high aerosol Fe flux observed during the spring season.

In terms of Fe inventories, the averaged dissolved Fe inventories were comparable between the summer and spring sampling periods, which were 54 and 46 μmol m^{-2}, respectively, using trapezoidal integration of the upper 150 m. The suspended particulate inventory in the spring was about 3-fold of the summer time in the top 150 m, which were 213 and 70 μmol m^{-2}, respectively. As the particulate P concentrations were comparable among the two sampling seasons (Table 2), the increase of suspended particulate Fe inventory in the surface water of the spring season was mainly attributed to aerosol input. Using Fe/P to be 7.5 mmol mol^{-1} as averaged intracellular Fe quota (Ho et al., 2003), intracellular Fe accounted for 20% of Fe in the total suspended particles for the summer period and only 3.3% for the spring period. As the medium size fraction is the dominant aerosol Fe fraction, in which most of the Fe are lithogenic particles (Figs. 3 and 5). These relatively large crystalline suspended lithogenic particles is supposed to sink out of the euphotic zone faster than smaller and less dense biotic particles. The precipitated and aggregated amorphous particulate Fe, such as iron oxides or oxyhydroxides (Kurisu et al., 2016), originated from soluble aerosol Fe may account for about 15%

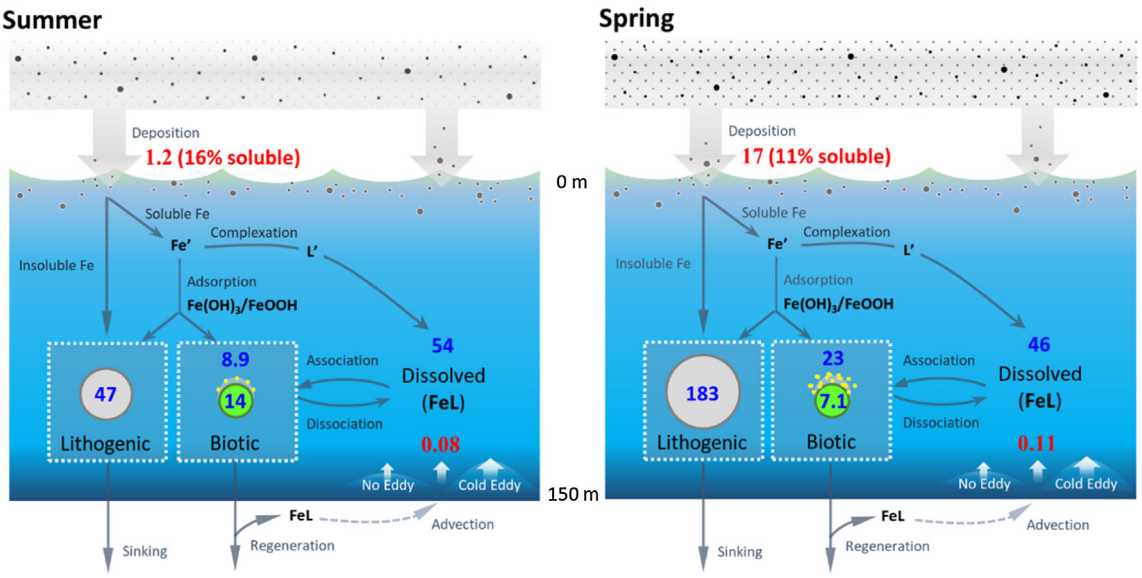

Fig. 5. Budgets of major Fe pools in the top 150 m of the studied region during the high and low aerosol deposition seasons. The budgets contain integrated dissolved and suspended particulate inventories (blue numbers) and averaged Fe input fluxes including aerosol deposition and upwelling (red numbers). The units of the fluxes and inventories are μmol m^{-2} d^{-1} and μmol m^{-2}, respectively. The biotic inventories are composed of two portions: the intracellular and extracellular aggregated fractions. The intracellular Fe inventories (numbers in green circles) are estimated by using intracellular Fe/P ratio (Ho et al., 2003) and averaged suspended particulate P of the three stations. The extracellular fraction (numbers above green circles) is labile abiotic fraction originated from aerosol soluble Fe, and suspended lithogenic inventories (numbers in grey circles) are remaining fraction after subtracting the labile abiotic fraction. The term, Association, stands for the combined processes of intracellular uptake, adsorption, and aggregation; and 'Dissociation' stands for the combined processes of degradation of biotic cells, desorption, disaggregation, and dissolution. (For interpretation of the references to color in this figure legend, the reader is referred to the web version of this article.)

abiotic Fe in the surface water by assuming most of the abiotic Fe originating from soluble Fe in aerosols. This amorphous particulate Fe may be defined as 'labile abiotic fraction' in the surface water as the amorphous Fe possesses much higher bioavailability and soluble tendency than crystalline Fe in lithogenic particles (Wells et al., 1983). Quantitatively, compared to the intracellular Fe fraction, the labile abiotic Fe fraction was relatively small for the summer season but was much larger than the intracellular pool during the spring period (Fig. 5). During high anthropogenic deposition period, the labile abiotic Fe on small size biotic particles may thus serve as major bioavailable Fe fraction in the euphotic zone. The labile pool increased significantly during high aerosol deposition season, increasing from 8.9 in the summer to 23 μmol m^{-2} in the spring (Fig. 5). In future studies, it is essential to quantify the labile abiotic fraction and to investigate its bioavailability and residence time in the euphotic zone.

In brief, most of biologically labile particulate Fe, including intracellular Fe and aggregated Fe from precipitated Fe, were in the small particles less than 2 μm. Fe in suspended particles larger than 2 μm were contributed mainly by medium size lithogenic particles, witnessed by the closeness of the Fe to Al ratios to the lithogenic ratios (Fig. S6). These seasonally specific elemental ratio patterns observed in size-fractionated particles reveal the distribution and roles of biotic and abiotic particulate Fe following aerosol Fe transformation in the surface ocean. Attributed to the physical, chemical, and biological property of the particles, intracellular Fe, extracellular aggregated Fe, and independent abiotic Fe particles shall undergo different cycling processes and possess different residence time and bioavailability in oceanic surface water.

5. Conclusions

Comprehensive sampling strategy for major Fe pools provides us the opportunity to investigate the transformation processes of aerosol Fe in the surface water of the NWPO. The comparable dissolved Fe concentrations among the two distinct aerosol deposition seasons reflect rapid precipitation and aggregation of aerosol soluble Fe, which resulted in significant elevation of suspended particulate Fe concentrations in the surface ocean during high aerosol deposition season. The elemental ratios of the suspended particulate Fe exhibited size-dependent distribution pattern, showing that the deposition of aerosol Fe mainly was transformed to abiotic suspended particles in sizes ranging from 2 to 25 μm in the surface water. This medium size lithogenic Fe fraction, with relatively large size and high density, should have much shorter residence time and less bioavailability than the labile particulate Fe associated with small biotic particles in the euphotic zone. The input of anthropogenic aerosols may thus significantly increase bioavailable Fe inventory in suspended particle pools during winter and spring monsoon seasons in the NWPO. The information of the labile Fe inventory in small biotic particles appears to be essential to understand the biogeochemical cycling of bioavailable Fe in the surface ocean with high aerosol deposition.

Declaration of Competing Interest

The authors declare that they have no known competing financial interests or personal relationships that could have appeared to influence the work reported in this paper.

Acknowledgements

We thank the staffs of R/V OR-5 and the hydrography team from TORI and NTU for their technical support during the cruises. We thank W.-H. Liao, H.-H. Yang, S.-C. Yang, C.-T. Chien, M.-C. Lu, S.-Y. Jiang, C.-P. Lee, V. Goswami, C. Chen, and J.-W. Chan for providing technical support and J.-H. Tai and G. S. Burr for their comments on this study. We thank the two anonymous reviewers for their helpful comments. The study was supported by the Ministry of Science and Technology with grant number 105-2119-M-001-039-MY3, 108-2611-M-001-006-MY3, and Career Development Award to T.-Y. Ho by the Academia Sinica.

Appendix A. Supplementary material

Supplementary data to this article can be found online at https://doi.org/10.1016/j.pocean.2020.102291.

References

Baker, A.R., Croot, P.L., 2010. Atmospheric and marine controls on aerosol iron solubility in seawater. Mar. Chem. 120, 4–13.

Baker, A.R., Jickells, T.D., 2006. Mineral particle size as a control on aerosol iron solubility. Geophys. Res. Lett. 33, L17608.

Benitez-Nelson, C.R., Bidigare, R.R., Dickey, T.D., Landry, M.R., Leonard, C.L., Brown, S.L., Nencioli, F., Rii, Y.M., Maiti, K., Becker, J.W., Bibby, T.S., Black, W., Cai, W.-J., Carlson, C.A., Chen, F., Kuwahara, V.S., Mahaffey, C., McAndrew, P.M., Quay, P.D., Rappé, M.S., Selph, K.E., Simmons, M.P., Yang, E.J., 2007. Mesoscale Eddies drive increased silica export in the subtropical pacific ocean. Science 316, 1017–1021.

Bentahila, Y., Ben Othman, D., Luck, J.-M., 2008. Strontium, lead and zinc isotopes in marine cores as tracers of sedimentary provenance: a case study around Taiwan orogen. Chem. Geol. 248, 62–82.

Bishop, J.K.B., 1999. Transmissometer measurement of POC. Deep Sea Res. Part I 46, 353–369.

Bowie, A.R., Townsend, A.T., Lannuzel, D., Remenyi, T.A., van der Merwe, P., 2010. Modern sampling and analytical methods for the determination of trace elements in marine particulate material using magnetic sector inductively coupled plasma–mass spectrometry. Anal. Chim. Acta 676, 15–27.

Bowie, A.R., van der Merwe, P., Quéroué, F., Trull, T., Fourquez, M., Planchon, F., Sarthou, G., Chever, F., Townsend, A.T., Obernosterer, I., Sallée, J.B., Blain, S., 2015. Iron budgets for three distinct biogeochemical sites around the Kerguelen Archipelago (Southern Ocean) during the natural fertilisation study, KEOPS-2. Biogeosciences 12, 4421–4445.

Boyd, P.W., Ellwood, M.J., Tagliabue, A., Twining, B.S., 2017. Biotic and abiotic retention, recycling and remineralization of metals in the ocean. Nat. Geosci. 10, 167–173.

Brown, M.T., Landing, W.M., Measures, C.I., 2005. Dissolved and particulate Fe in the western and central North Pacific: Results from the 2002 IOC cruise. Geochem. Geophys. Geosyst. 6, 1–20.

Buck, C.S., Landing, W.M., Resing, J., 2013. Pacific Ocean aerosols: deposition and solubility of iron, aluminum, and other trace elements. Mar. Chem. 157, 117–130.

Buck, C.S., Landing, W.M., Resing, J.A., Lebon, G.T., 2006. Aerosol iron and aluminum solubility in the northwest Pacific Ocean: Results from the 2002 IOC cruise. Geochem. Geophys. Geosyst. 7, Q04M07.

Chen, K.-S., Hung, C.-C., Gong, G.-C., Chou, W.-C., Chung, C.-C., Shih, Y.-Y., Wang, C.-C., 2013. Enhanced POC export in the oligotrophic northwest Pacific Ocean after extreme weather events. Geophys. Res. Lett. 40, 5728–5734.

Chuang, P.Y., Duvall, R.M., Shafer, M.M., Schauer, J.J., 2005. The origin of water soluble particulate iron in the Asian atmospheric outflow. Geophys. Res. Lett. 32, L07813.

Collier, R., Edmond, J., 1984. The trace element geochemistry of marine biogenic particulate matter. Prog. Oceanogr. 13, 113–199.

Conway, T.M., Hamilton, D.S., Shelley, R.U., Aguilar-Islas, A.M., Landing, W.M., Mahowald, N.M., John, S.G., 2019. Tracing and constraining anthropogenic aerosol iron fluxes to the North Atlantic Ocean using iron isotopes. Nat. Commun. 10, 2628.

Duce, R.A., Tindale, N.W., 1991. Atmospheric transport of iron and its deposition in the ocean. Limnol. Oceanogr. 36, 1715–1726.

Faul, K.L., Paytan, A., Delaney, M.L., 2005. Phosphorus distribution in sinking oceanic particulate matter. Mar. Chem. 97, 307–333.

Fitzsimmons, J.N., Boyle, E.A., 2014. Both soluble and colloidal iron phases control dissolved iron variability in the tropical North Atlantic Ocean. Geochim. Cosmochim. Acta 125, 539–550.

Fung, I.Y., Meyn, S.K., Tegen, I., Doney, S.C., John, J.G., Bishop, J.K.B., 2000. Iron supply and demand in the upper ocean. Global Biogeochem. Cycles 14, 281–295.

Hansard, S.P., Landing, W.M., Measures, C.I., Voelker, B.M., 2009. Dissolved iron(II) in the Pacific Ocean: measurements from the PO2 and P16N CLIVAR/CO2 repeat hydrography expeditions. Deep Sea Res. Part I 56, 1117–1129.

Hirose, K., Kamiya, H., 2003. Vertical nutrient distributions in the Western North Pacific Ocean: simple model for estimating nutrient upwelling, export flux and consumption rates. J. Oceanogr. 59, 149–161.

Ho, T.-Y., 2006. The trace metal composition of marine microalgae in cultures and natural assemblages. In: Subba Rao, D.V. (Ed.), Algal Cultures: Analogues of Blooms and Applications. Science Publishers, pp. 271–299.

Ho, T.-Y., Chou, W.-C., Lin, H.-L., Sheu, D.D., 2011. Trace metal cycling in the deep water of the South China Sea: the composition, sources, and fluxes of sinking particles. Limnol. Oceanogr. 56, 1225–1243.

Ho, T.-Y., Chou, W.-C., Wei, C.-L., Lin, F.-J., Wong, G.T.F., Line, H.-L., 2010. Trace metal cycling in the surface water of the South China Sea: vertical fluxes, composition, and sources. Limnol. Oceanogr. 55, 1807–1820.

Ho, T.-Y., Quigg, A., Finkel, Z.V., Milligan, A.J., Wyman, K., Falkowski, P.G., Morel, F.M.M., 2003. The elemental composition of some marine phytoplankton. J. Phycol. 39, 1145–1159.

Ho, T.-Y., Tu, W.-C., Hsieh, C.-C., Yang, S.-C., Liao, W.-H., 2018. Anthropogenic aerosols: The major source of soluble iron in the surface water of the northwestern Pacific Ocean. Ocean Science Meeting. Portland, Oregon, USA.

Ho, T.-Y., Wen, L.-S., You, C.-F., Lee, D.-C., 2007. The trace metal composition of size-fractionated plankton in the South China Sea: biotic versus abiotic sources. Limnol. Oceanogr. 52, 1776–1788.

Hunter, K.A., Boyd, P.W., 2007. Iron-binding ligands and their role in the ocean biogeochemistry of iron. Environ. Chem. 4, 221–232.

Jickells, T.D., An, Z.S., Andersen, K.K., Baker, A.R., Bergametti, G., Brooks, N., Cao, J.J., Boyd, P.W., Duce, R.A., Hunter, K.A., Kawahata, H., Kubilay, N., laRoche, J., Liss, P.S., Mahowald, N., Prospero, J.M., Ridgwell, A.J., Tegen, I., Torres, R., 2005. Global iron connections between desert dust, ocean biogeochemistry, and climate. Science 308, 67–71.

Johnson, K.S., Elrod, V.A., Fitzwater, S.E., Plant, J.N., Chavez, F.P., Tanner, S.J., Gordon, R.M., Westphal, D.L., Perry, K.D., Wu, J., Karl, D.M., 2003. Surface ocean-lower atmosphere interactions in the Northeast Pacific Ocean Gyre: aerosols, iron, and the ecosystem response. Global Biogeochem. Cycles 17, 1063.

Kurisu, M., Takahashi, Y., Iizuka, T., Uematsu, M., 2016. Very low isotope ratio of iron in fine aerosols related to its contribution to the surface ocean. J. Geophys. Res.: Atmosph. 121, 11,119–111,136.

Lam, P.J., Ohnemus, D.C., Auro, M.E., 2015. Size-fractionated major particle composition and concentrations from the US GEOTRACES North Atlantic Zonal Transect. Deep Sea Res. Part II 116, 303–320.

Liao, W.-H., Yang, S.-C., Ho, T.-Y., 2017. Trace metal composition of size-fractionated plankton in the Western Philippine Sea: the impact of anthropogenic aerosol deposition. Limnol. Oceanogr. 62, 2243–2259.

Lin, Y.-C., Chen, J.-P., Ho, T.-Y., Tsai, I.C., 2015. Atmospheric iron deposition in the northwestern Pacific Ocean and its adjacent marginal seas: the importance of coal burning. Global Biogeochemical Cycles 2013GB004795.

Liu, X., Millero, F.J., 2002. The solubility of iron in seawater. Mar. Chem. 77, 43–54.

Luo, C., Mahowald, N., Bond, T., Chuang, P.Y., Artaxo, P., Siefert, R., Chen, Y., Schauer, J., 2008. Combustion iron distribution and deposition. Global Biogeochem. Cycles 22, GB1012.

Martin, J.H., Coale, K.H., Johnson, K.S., Fitzwater, S.E., Gordon, R.M., Tanner, S.J., Hunter, C.N., Elrod, V.A., Nowicki, J.L., Coley, T.L., Barber, R.T., Lindley, S., Watson, A.J., Van Scoy, K., Law, C.S., Liddicoat, M.I., Ling, R., Stanton, T., Stockel, J., Collins, C., Anderson, A., Bidigare, R., Ondrusek, M., Latasa, M., Millero, F.J., Lee, K., Yao, W., Zhang, J.Z., Friederich, G., Sakamoto, C., Chavez, F., Buck, K., Kolber, Z., Greene, R., Falkowski, P., Chisholm, S.W., Hoge, F., Swift, R., Yungel, J., Turner, S., Nightingale, P., Hatton, A., Liss, P., Tindale, N.W., 1994. Testing the iron hypothesis in ecosystems of the equatorial Pacific Ocean. Nature 371, 123–129.

Martin, J.H., Knauer, G.A., 1973. The elemental composition of plankton. Geochim. Cosmochim. Acta 37, 1639–1653.

Matsui, H., Koike, M., Kondo, Y., Oshima, N., Moteki, N., Kanaya, Y., Takami, A., Irwin, M., 2013. Seasonal variations of Asian black carbon outflow to the Pacific: contribution from anthropogenic sources in China and biomass burning sources in Siberia and Southeast Asia. J. Geophys. Res.: Atmosph. 118, 9948–9967.

Morton, P.L., 2010. Trace Metal Biogeochemistry in the Western North Pacific Vol. PhD Old Dominion University, Norfolk, VA.

Morton, P.L., Landing, W.M., Hsu, S.C., Milne, A.M.A.-I.A., Baker, A.R., Bowie, A.R., Buck, C.S., Gao, Y., Gichuki, S., Hastings, M.G., Hatta, M., Johansen, A.M., Losno, R., Mead, C., Patey, M.D., Swarr, G., Vandermark, A., Zamora, L.M., 2013. Methods for the sampling and analysis of marine aerosols: results from the 2008 GEOTRACES aerosol intercalibration experiment. Limnol. Oceanogr. 11, 62–78.

Myhre, G., Berglen, T.F., Johnsrud, M., Hoyle, C.R., Berntsen, T.K., Christopher, S.A., Fahey, D.W., Isaksen, I.S.A., Jones, T.A., Kahn, R.A., Loeb, N., Quinn, P., Remer, L., Schwarz, J.P., Yttri, K.E., 2009. Modelled radiative forcing of the direct aerosol effect with multi-observation evaluation. Atmos. Chem. Phys. 9, 1365–1392.

Nuester, J., Vogt, S., Newville, M., Kustka, A.B., Twining, B.S., 2012. The unique biogeochemical signature of the marine diazotroph trichodesmium. Front. Microbiol. 3, 150.

Park, S.-U., Lee, I.-H., Joo, S.J., 2016. Spatial and temporal distributions of aerosol concentrations and depositions in Asia during the year 2010. Sci. Total Environ. 542, 210–222.

Partensky, F., Hess, W.R., Vaulot, D., 1999. Prochlorococcus, a marine photosynthetic prokaryote of global significance. Microbiol. Mol. Biol. Rev. 63, 106–127.

Planquette, H., Sherrell, R.M., 2012. Sampling for particulate trace element determination using water sampling bottles: methodology and comparison to in situ pumps. Limnol. Oceanogr. Methods 10, 367–388.

Planquette, H., Sherrell, R.M., Stammerjohn, S., Field, M.P., 2013. Particulate iron delivery to the water column of the Amundsen Sea, Antarctica. Mar. Chem. 153, 15–30.

Sarthou, G., Baker, A.R., Blain, S., Achterberg, E.P., Boye, M., Bowie, A.R., Croot, P., Laan, P., de Baar, H.J.W., Jickells, T.D., Worsfold, P.J., 2003. Atmospheric iron deposition and sea-surface dissolved iron concentrations in the eastern Atlantic Ocean. Deep Sea Res. Part I 50, 1339–1352.

Schlitzer, R., Anderson, R.F., Dodas, E.M., Lohan, M., Geibert, W., Tagliabue, A., Bowie, A., Jeandel, C., Maldonado, M.T., Landing, W.M., Cockwell, D., Abadie, C., Abouchami, W., Achterberg, E.P., Agather, A., Aguliar-Islas, A., van Aken, H.M., Andersen, M., Archer, C., Auro, M., de Baar, H.J., Baars, O., Baker, A.R., Bakker, K., Basak, C., Baskaran, M., Bates, N.B., Bauch, D., van Beek, P., Behrens, M.K., Black, E., Bluhm, K., Bopp, L., Bouman, H., Bowman, K., Bown, J., Boyd, P., Boye, M., Boyle, E.A., Branellec, P., Bridgestock, L., Brissebrat, G., Browning, T., Bruland, K.W., Brumsack, H.-J., Brzezinski, M., Buck, C.S., Buck, K.N., Buesseler, K., Bull, A., Butler, E., Cai, P., Mor, P.C., Cardinal, D., Carlson, C., Carrasco, G., Casacuberta, N., Casciotti, K.L., Castrillejo, M., Chamizo, E., Chance, R., Charette, M.A., Chaves, J.E., Cheng, H., Chever, F., Christl, M., Church, T.M., Closset, I., Colman, A., Conway, T.M., Cossa, D., Croot, P., Cullen, J.T., Cutter, G.A., Daniels, C., Dehairs, F., Deng, F., Dieu, H.T., Duggan, B., Dulaquais, G., Dumousseaud, C., Echegoyen-Sanz, Y., Edwards, R.L., Ellwood, M., Fahrbach, E., Fitzsimmons, J.N., Flegal, A.R., Fleisher, M.Q., van de Flierdt, T., Frank, M., Friedrich, J., Fripiat, F., Fröllje, H., Galer, S.J.G., Gamo, T., Ganeshram, R.S., Garcia-Orellana, J., Garcia-Solsona, E., Gault-Ringold, M., George, E., Gerringa, L.J.A., Gilbert, M., Godoy, J.M., Goldstein, S.L., Gonzalez, S.R., Grissom, K., Hammerschmidt, C., Hartman, A., Hassler, C.S., Hathorne, E.C.,

Hatta, M., Hawco, N., Hayes, C.T., Heimbürger, L.-E., Helgoe, J., Heller, M., Henderson, G.M., Henderson, P.B., van Heuven, S., Ho, P., Horner, T.J., Hsieh, Y.-T., Huang, K.-F., Humphreys, M.P., Isshiki, K., Jacquot, J.E., Janssen, D.J., Jenkins, W.J., John, S., Jones, E.M., Jones, J.L., Kadko, D.C., Kayser, R., Kenna, T.C., Khondoker, R., Kim, T., Kipp, L., Klar, J.K., Klunder, M., Kretschmer, S., Kumamoto, Y., Laan, P., Labatut, M., Lacan, F., Lam, P.J., Lambelet, M., Lamborg, C.H., Le Moigne, F.A.C., Le Roy, E., Lechtenfeld, O.J., Lee, J.M., Lherminier, P., Little, S., López-Lora, M., Lu, Y., Masque, P., Mawji, E., Mcclain, C.R., Measures, C., Mehic, S., Barraqueta, J.-L.M., van der Merwe, P., Middag, R., Mieruch, S., Milne, A., Minami, T., Moffett, J.W., Moncoiffe, G., Moore, W.S., Morris, P.J., Morton, P.L., Nakaguchi, Y., Nakayama, N., Niedermiller, J., Nishioka, J., Nishiuchi, A., Noble, A., Obata, H., Ober, S., Ohnemus, D.C., van Ooijen, J., O'Sullivan, J., Owens, S., Pahnke, K., Paul, M., Pavia, F., Pena, L.D., Peters, B., Planchon, F., Planquette, H., Pradoux, C., Puigcorbé, V., Quay, P., Queroue, F., Radic, A., Rauschenberg, S., Rehkämper, M., Rember, R., Remenyi, T., Resing, J.A., Rickli, J., Rigaud, S., Rijkenberg, M.J.A., Rintoul, S., Robinson, L.F., Roca-Martí, M., Rodellas, V., Roeske, T., Rolison, J.M., Rosenberg, M., Roshan, S., van der Loeff, M.M.R., Ryabenko, E., Saito, M.A., Salt, L.A., Sanial, V., Sarthou, G., Schallenberg, C., Schauer, U., Scher, H., Schlosser, C., Schnetger, B., Scott, P., Sedwick, P.N., Semiletov, I., Shelley, R., Sherrell, R.M., Shiller, A.M., Sigman, D.M., Singh, S.K., Slagter, H.A., Slater, E., Smethie, W.M., Snaith, H., Sohrin, Y., Sohst, B., Sonke, J.E., Speich, S., Steinfeldt, R., Stewart, G., Stichel, T., Stirling, C.H., Stutsman, J., Swarr, G.J., Swift, J.H., Thomas, A., Thorne, K., Till, C.P., Till, R., Townsend, A.T., Townsend, E., Tuerena, R., Twining, B.S., Vance, D., Velazquez, S., Venchiarutti, C., Villa-Alfageme, M., Vivancos, S.M., Voelker, A.H.L., Wake, B., Warner, M.J., Watson, R., van Weerlee, E., Weigand, M.A., Weinstein, Y., Weiss, D., Wisotzki, A., Woodward, E.M.S., Wu, J., Wu, Y., Wuttig, K., Wyatt, N., Xiang, Y., Xie, R.C., Xue, Z., Yoshikawa, H., Zhang, J., Zhang, P., Zhao, Y., Zheng, L., Xin-Yuan Zheng, X.-Y., Zieringer, M., Zimmer, Louise A., Ziveri, P., Zunino, P., Zurbrick, C., 2018. The GEOTRACES intermediate data product 2017. Chem. Geol. 493, 210–223.

Schroth, A.W., Crusius, J., Sholkovitz, E.R., Bostick, B.C., 2009. Iron solubility driven by speciation in dust sources to the ocean. Nat. Geosci. 2, 337–340.

Sherrell, R., Twining, B., German, C., 2016. Trace elements in suspended particles from GO-Flo bottles. Biological and Chemical Oceanography Data Management Office (BCO-DMO) Dataset version 2016-05-17, http://lod.bco-dmo.org/id/dataset/639847 [May 639801, 632018].

Shih, Y.-Y., Hung, C.-C., Gong, G.-C., Chung, W.-C., Wang, Y.-H., Lee, I.H., Chen, K.-S., Ho, C.-Y., 2015. Enhanced particulate organic carbon export at eddy edges in the oligotrophic Western North Pacific Ocean. PLoS ONE 10.

Sholkovitz, E.R., Sedwick, P.N., Church, T.M., Baker, A.R., Powell, C.F., 2012. Fractional solubility of aerosol iron: Synthesis of a global-scale data set. Geochim. Cosmochim. Acta 89, 173–189.

Tagliabue, A., Bowie, A.R., Boyd, P.W., Buck, K.N., Johnson, K.S., Saito, M.A., 2017. The integral role of iron in ocean biogeochemistry. Nature 543, 51.

Takahashi, Y., Higashi, M., Furukawa, T., Mitsunobu, S., 2011. Change of iron species and iron solubility in Asian dust during the long-range transport from western China to Japan. Atmos. Chem. Phys. 11, 11237–11252.

Tovar-Sanchez, A., Sañudo-Wilhelmy, S.A., Kustka, A.B., Agustí, S., Dachs, J., Hutchins, D.A., Capone, D.G., Duarte, C.M., 2006. Effects of dust deposition and river discharges on trace metal composition of Trichodesmium spp. in the tropical and subtropical North Atlantic Ocean. Limnol. Oceanogr. 51, 1755–1761.

Twining, B.S., Baines, S.B., Bozard, J.B., Vogt, S., Walker, E.A., Nelson, D.M., 2011. Metal quotas of plankton in the equatorial Pacific Ocean. Deep Sea Res. Part II 58, 325–341.

Twining, B.S., Rauschenberg, S., Morton, P.L., Vogt, S., 2015. Metal contents of phytoplankton and labile particulate material in the North Atlantic Ocean. Prog. Oceanogr. 137, 261–283.

Twining, B.S., Sherrell, R.M., German, C., 2016. Trace elements in suspended particles from GO-Flo bottles. Biological and Chemical Oceanography Data Management Office (BCO-DMO). Dataset version 2016-05-17. http://lod.bco-dmo.org/id/dataset/639847. Access date: April 16, 2018.

Uematsu, M., Wang, Z., Uno, I., 2003. Atmospheric input of mineral dust to the western North Pacific region based on direct measurements and a regional chemical transport model. Geophys. Res. Lett. 30, 1342.

Wang, B.-S., Lee, C.-P., Ho, T.-Y., 2014. Trace metal determination in natural waters by automated solid phase extraction system and ICP-MS: the influence of low level Mg and Ca. Talanta 128, 337–344.

Wedepohl, K.H., 1995. The composition of the continental crust. Geochim. Cosmochim. Acta 59, 1217–1232.

Weinstein, S.E., Moran, S.B., 2004. Distribution of size-fractionated particulate trace metals collected by bottles and in-situ pumps in the Gulf of Maine-Scotian Shelf and Labrador Sea. Mar. Chem. 87, 121–135.

Wells, M.L., Zorkin, N.G., Lewis, A.G., 1983. The role of colloid chemistry in providing a source of iron to phytoplankton. J. Mar. Res. 41, 731–746.

Wilhelm, S.W., King, A.L., Twining, B.S., LeCleir, G.R., DeBruyn, J.M., Strzepek, R.F., Breene, C.L., Pickmere, S., Ellwood, M.J., Boyd, P.W., Hutchins, D.A., 2013. Elemental quotas and physiology of a southwestern Pacific Ocean plankton community as a function of iron availability. Aquat. Microb. Ecol. 68, 185–194.

Wu, J., Wells, M.L., Rember, R., 2011. Dissolved iron anomaly in the deep tropical–subtropical Pacific: evidence for long-range transport of hydrothermal iron. Geochim. Cosmochim. Acta 75, 460–468.

Yiğiterhan, O., Murray, J.W., Tuğrul, S., 2011. Trace metal composition of suspended particulate matter in the water column of the Black Sea. Mar. Chem. 126, 207–228.

Young, J.A., Silker, W.B., 1980. Aerosol deposition velocities on the Pacific and Atlantic oceans calculated from7Be measurements. Earth Planet. Sci. Lett. 50, 92–104.